



UNIVERSITY OF  
GLOUCESTERSHIRE

This is a peer-reviewed, post-print (final draft post-refereeing) version of the following published document, © 2019 Society of Plastics Engineers This is the peer reviewed version of the following article: Mensler, Holger, Zhang, Shujun and Win, Thu Yein (2019) A Method for Determining the Flow Front Velocity of a Plastic Melt in an Injection Molding Process. Polymer Engineering and Science, 59 (6). pp. 1132-1145. ISSN 0032-3888, which has been published in final form at <https://doi.org/10.1002/pen.25092>. This article may be used for non-commercial purposes in accordance with Wiley Terms and Conditions for Use of Self-Archived Versions. and is licensed under All Rights Reserved license:

**Mensler, Holger, Zhang, Shujun ORCID logoORCID:  
<https://orcid.org/0000-0001-5699-2676> and Win, Thu Yein  
ORCID logoORCID: <https://orcid.org/0000-0002-4977-0511>  
(2019) A Method for Determining the Flow Front Velocity of a  
Plastic Melt in an Injection Molding Process. Polymer  
Engineering and Science, 59 (6). pp. 1132-1145.  
[doi:10.1002/pen.25092](https://doi.org/10.1002/pen.25092)**

Official URL: <https://doi.org/10.1002/pen.25092>  
DOI: <http://dx.doi.org/10.1002/pen.25092>  
EPrint URI: <https://eprints.glos.ac.uk/id/eprint/6727>

#### **Disclaimer**

The University of Gloucestershire has obtained warranties from all depositors as to their title in the material deposited and as to their right to deposit such material.

The University of Gloucestershire makes no representation or warranties of commercial utility, title, or fitness for a particular purpose or any other warranty, express or implied in respect of any material deposited.

The University of Gloucestershire makes no representation that the use of the materials will not infringe any patent, copyright, trademark or other property or proprietary rights.

The University of Gloucestershire accepts no liability for any infringement of intellectual property rights in any material deposited but will remove such material from public view pending investigation in the event of an allegation of any such infringement.

PLEASE SCROLL DOWN FOR TEXT.

# A Method for Determining the Flow Front Velocity of a Plastic Melt in an Injection Molding Process

Holger Mensler <sup>1</sup>, Shujun Zhang,<sup>2</sup> Thomas Win<sup>2</sup>

<sup>1</sup>Oetzstrasse 1a, D-83730, Fischbachau, Germany

<sup>2</sup>School of Computing and Technology, University of Gloucestershire, the Park, Cheltenham, GL50 2RH, UK

**During the filling phase of an injection molding process, the flow front velocity of the plastics melt has a decisive influence on the form part quality. It has been believed that a constant flow front velocity of the melt leads to distortion-free and residual stress-free form parts. A process control strategy based on a constant flow front velocity of the melt, however, requires the full understanding of the flow front position as a function of the screw position of the injection molding machine. With current methods, this can only be achieved by direct measurements using a number of sensors inside the mold, which leads to complicated structure, great efforts, and high cost for the tooling equipment. This article proposes, designs, and develops an innovative method for determining the flow front velocity of a plastic melt in an injection molding using only one pressure sensor at the front of the screw and based on the idea of mapping a simulated filling process to a real injection molding process. The mapping ensues that the characteristic event points are identified and matched for both the simulated and real filling process. The results of the simulation analysis and experimental evaluation show that the proposed method can be used to determine the flow front position and the resulting flow front velocity of the melt within the cavity of the mold and provide evidence that the new method offers great potential to process control strategies based on machine independent parameters. POLYM. ENG. SCI., 00:000–000, 2019. © 2019 Society of Plastics Engineers**

## INTRODUCTION

Even though the development and use of generative manufacturing processes has accelerated disproportionately in recent years, “injection molding” will remain the dominant process for mass-production of plastic parts for the foreseeable future. As in the entire industry, this manufacturing process is subject to the trend to ever higher requirements in relation to quality, tolerances, and manufacturing costs on form parts. Despite state-of-the-art injection, molding machines can be used to produce a high level of repeatability from shot to shot and offering users a variety of quality monitoring options, the situation in the past—and still applicable today—has nevertheless been characterized by the fact that a constant form part quality is largely derived from the machine setup [1]. This setting of the injection and holding pressure stages has been studied thoroughly by Chen [2] and many approaches by researchers have been made to monitor and dynamic control the quality stability of the injection molding process [3, 4]. Only recently, and with the development of new methods for determining the flow front velocity of the melt in a flow channel [5, 6], the recognition prevails that the quality defining parameters are

independent of the machine [7]. As Bader describes a future scenario that in an intelligent way, the mold and not the machine controls the injection molding process is conceivable. Machine-independent parameters, such as the flow front velocity and the melt viscosity at specific flow-path sections will act as control variables. The machine-setting parameters will become dependent variables. In this regard, it is “immaterial” to the mold, on what machine it runs, provided that the required parameters can be achieved.

Injection molding is a cyclic process in which molten plastic material is injected into a mold cavity and solidifies under pressures into usable form parts of different geometries [8]. The filling phase of the process is characterized by high flow rates and hence high shear rates of the polymer [9, 10]. Due to the rapid filling, heat is generated by viscous dissipation depending on both the viscosity and the shear rate of the resin. So, the relationship between the process variables and the form part quality is complicated. In practice, it is very difficult to gain a full understanding of the relationship between preset parameters and the form part quality without the knowledge of the flow pattern of the melt within the mold cavity [11]. The form part quality is significantly affected by the flow pattern and the injection rate [12, 13]. The injection rate is related to the forward speed of the injection piston of the screw and can vary during the filling phase. It is a fundamental process parameter in the setting (setup) of the injection molding machine and thus the optimization of the molding process. During machine setup, an injection rate profile of injection speed over the screw stroke is entered into the machine control unit by operators [8, 9].

Researchers in injection molding area [2, 14–17] have all recommended that an approximately constant flow front velocity of the melt on its entire flow path leads to optimized residual stress and homogenous form parts. Another, by Bader suggested, control strategy for continuously achieving a high surface quality is to keep the melt viscosity constant during injection [7].

The problem is how to find a suitable injection rate profile that meets the above requirement [12, 18]. In practice, the setting of the injection molder is still largely empirical and follows a similar pattern that the machine operator “performs a basic setting” and then optimizes the molded part “on the basis of experience.” However, when being asked to describe their “experience,” operators regularly come up to limits. Only in the rarest cases, a clearly ruled-based optimization strategy has been followed.

The reason for this is that optimization strategies require full understanding of the flow front position and its velocity in relation to the screw position along the entire flow path of the cavity. Zhou [19], for example, believes that even though injection speed can be accurately closed-loop controlled with good robustness, the setting of the injection speed profile remains a difficult task. He raises the question of how the injection speed should be profiled to produce parts with even distributed quality. He also thinks that there is a lack of methods for practically and effectively measuring melt flow front position and velocity.

Correspondence to: H. Mensler: e-mail: hmensler@aol.com

DOI 10.1002/pen.25092

Published online in Wiley Online Library (wileyonlinelibrary.com).

© 2019 Society of Plastics Engineers

Figure 1 shows the relationships between the injection speed  $v_b$  (with the screw cross-sectional area  $A_b$  and the screw position  $x_b$ ) and the melt flow front velocity  $v_m$  (with the cross-sectional area of the flow channel  $A_m$  at the position  $x_m$ ). It is obvious that the flow front position and the flow front velocity depend on the flow channel geometry. Only in the rarest cases, the cavity fills along a single flow path (one-dimensional). For such simple geometries, Gao and coworkers have developed a transducer to measure the melt front position directly [20]. The sensor output is linear to the melt front position. However, usually with complex geometries, the form part fills over all three spatial directions depending on location and time.

The problem is that at present and under real production conditions with complex part geometries, the relationship between screw position and melt front velocity can only be determined using at least two or more sensors installed along the flow path to measure the positions of the melt front in relation to injection time and/or position of the screw [5, 6]. Although such systems for the direct measurement of the melt front position by two or more sensors inside the mold have been studied and are occasionally adopted with some levels of success, they have not been widely applied in injection plastic molding. The biggest problem associated with the direct measurement method is that the flow front position and all derived parameters, such as velocity and viscosity, can only be determined in the limited spaces between the successive two sensor positions. Continuous measurement over the entire flow path is practically impossible. Furthermore, there are also other problems associated with system design and form part quality. On the one hand, it is often too complicated to place more sensors in the limited space along the flow path and the installation of the sensors significantly reduce the stiffness of the mold and/or its ability for the part surface to cool down uniformly. On the other hand, the equipping and retrofitting of the mold is very time-consuming and expensive. So, the direct measurement method is not suitable to many practical applications.

From a kinematics point of view, the flow front velocity can be determined using the flow front position [5, 6, 21, 22]. So, if the relationship between the flow front position and the screw position can be established, then the relationship between the flow front velocity and the screw position can be established and thus the problem to find a suitable injection rate profile can be solved.

To solve the above problems, this article proposes, designs, and develops a new method for determining the flow front velocity as a function of the screw position over the entire part geometry using only one sensor for an advanced controlling strategy with practical application values.

## PROPOSITION OF THE NEW METHOD FOR DETERMINING THE FLOW FRONT VELOCITY

The proposed new method is based on the understanding that it is possible to isolate “singular events” using the part geometry and numerical simulation results of a mold filling process. A singular event is defined as an individual event when the melt front has a particular characteristic at a position within the cavity. In this definition, the relationship is established between the time when a singular event happens and the associated position within the cavity.

The part geometry normally changes along the flow path of the melt. The geometrical changes occur at tapering, enlargements, edges, corners and flow obstacles, and so forth. It is widely accepted that these changes result in a significant change of the melt pressure during the flow through of the melt [9, 23]. In this article, these positions are defined as “event points”  $F$ . Correspondingly, a singular event, denoted by  $E$ , occurs. Singular events can occur in the form of “event groups.” The sequence of all events can be analyzed to identify a pattern of the form part. This pattern is called the “form part-specific event pattern”  $M_s$  and can be considered as the “fingerprint” of the form part.

In this article, two kinds of singular events will be used: one is for the events identified through simulation analysis and the other is for the events identified through experimental measurements. The events through simulation analysis are called virtual singular events  $E_{sim}$  and they can be determined from a melt pressure curve generated from simulation analysis. Similarly, the events identified through the experimental measurement are called real singular events  $E_{mach}$  and they can be determined from a pressure curve measured at a location such as in the nozzle of the injection unit. A number of virtual singular events form a virtual form part-specific event pattern,  $M_s$  and a number of real singular events form a real event pattern,  $M_m$ .

To determine the flow front velocity in relation to the position of the screw, a new method is proposed by comparative analysis of the above two event patterns. There are three stages consisting of a total of 14 steps in the proposed method as shown in Fig. 2.

### Stage 1: Form Part-Specific Event Pattern

In this stage, the form part-specific event pattern will be determined in the first five steps.

In Step 1, the all required geometric data of the form part are fully captured. They usually exist in the form of machine-readable data for example in form of a step file (.stp).

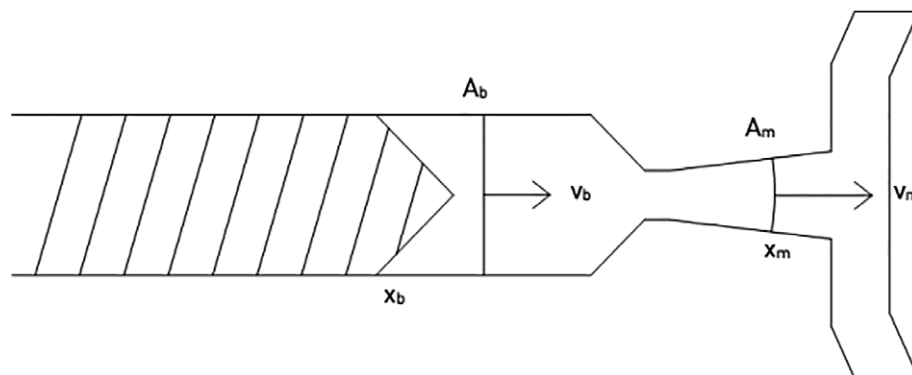


FIG. 1. Relation of screw position and flow front velocity.

In Step 2, the data of the gating system are obtained.

In Step 3, using the geometric data, a simulation of the filling process can be performed to determine the form part-specific pressure curve  $p_{sim}$ . This form part-specific pressure curve (Fig. 3) defines the melt pressure during filling phase over a period of time  $t_{sim}$ , which represents the injection time in relation to a specific start time. This start time can, for example, be defined as the time when the melt front enters the sprue channel or passes the gate of the cavity.

Figure 4 shows how the time can be determined when virtual events  $E_{sim 1}$ ,  $E_{sim 2}$ , and  $E_{sim 3}$  occur by the analysis of the differentiated form part-specific pressure curve (Step 4). It can be observed that the pressure gradient changes from a relatively less slope section to deep slope section. Two tangent lines can be determined for each section. Then, the cross point of these two tangent lines can be determined. The vertical line can be drawn through this cross point. The intersection of this vertical line with horizontal axis (time) can be defined as the time of each respective event. For example, three events can be identified, as shown in Fig. 4.

This form part-specific event pattern can be represented using the expression  $M_s (E_{sim 1}, \dots, E_{sim n})$ .

This event pattern consists of  $n$  virtual events  $E_{sim i}$ , which are associated with the characteristic event points of the part geometry. Each virtual event is assigned to a relative time when the

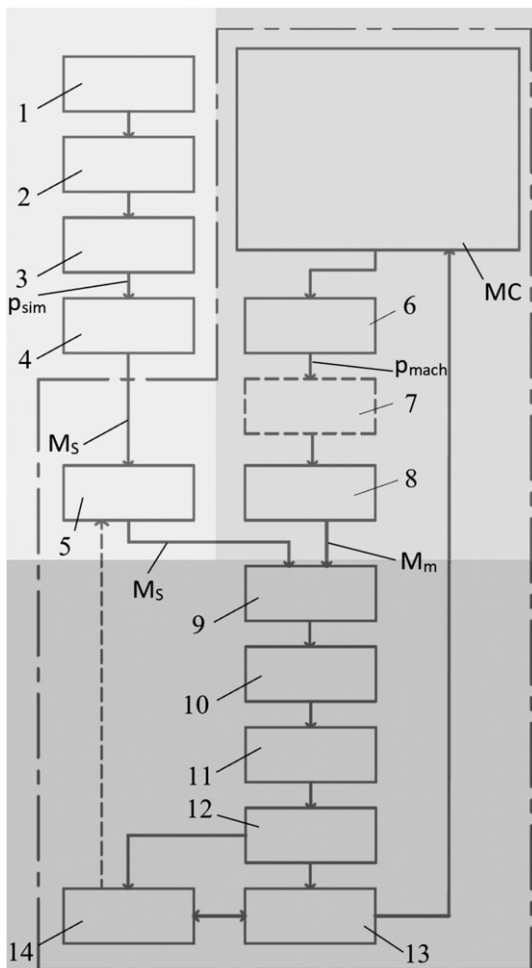


FIG. 2. Flowchart of the proposed method.

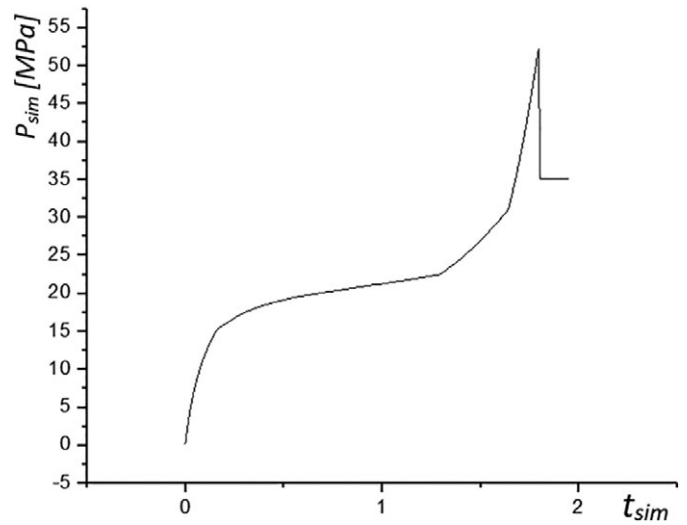


FIG. 3. Form part-specific pressure curve.

event happens and the associated position. This can be a simple information on the position if only a one-dimensional flow path is considered. In a finite element network, these are the positions of all nodes, along which the melt front lies at the time of the event.

$E_{sim i} (t_{sim i}, x_{sim i}, y_{sim i}, z_{sim i}, p_{sim i}, h_{sim i})$  is thus a vector, which—in addition to the event time  $t_{sim i}$ —also includes other components: a position data, respectively, represent the positions of the melt front  $X_{sim i}$ ,  $Y_{sim i}$ ,  $Z_{sim i}$  as information on the form part geometry  $h_{sim i}$  at the event location. Plotted against time, all events form an individual and unique form part-specific event pattern  $M_s$  (Fig. 5). The pattern describes the relative assignment of all events occurring during a virtual filling phase and is considered as the fingerprint of the form part.

In Step 5, the form part-specific pattern  $M_s$ , the geometry data and the other data such as the filling pattern obtained through the simulation analysis, are uploaded into the control unit of the injection molding machine.

#### Stage 2: Identification of Real Event Pattern

Stage 2 consists of three steps: Steps 6–8. In Stage 2, the real event pattern is identified.

Modern injection molding machines are able to control parameters such as temperatures, pressures, and velocities within narrow

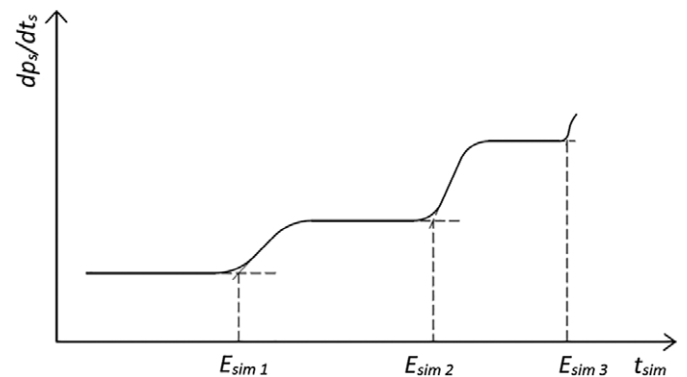


FIG. 4. Three events can be identified from a numerical calculated pressure in accordance with the virtual time.

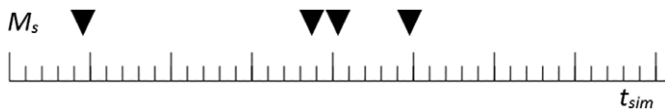


FIG. 5. Form part-specific event pattern  $M_s$ .

limits. The machine controller compares a set of parameters with the measured data and then acts on built-in or external actuators. With close loop-controlled injection, the melt pressure is a function of the injection rate. For each cycle, the count of the machine time  $t_m$  starts, for example, at the beginning of the injection process.

When the plastics melt passes through the cavity, the resulting pressure to overcome the filling resistance can be directly or indirectly measured as a function of the machine time and the position of the screw. For the direct acquisition of the signal, the measurement is done using pressure sensors inside the melt, for example, in the nozzle of the injection unit. For the indirect measurement, the melt pressure signal is derived from the hydraulic pressure of the injection piston or the torque of the electric driven injection unit.

In Step 6, the pressure measurement is carried out to obtain the melt pressure curve  $p_{mach}$ . Figure 6 shows a typical measured curve which can optionally be adjusted in Step 7. This may be necessary if the volumetric flow rate  $\dot{V}$  is not kept constant during injection as in the simulation. Using the data on the change in the flow rate, a conversion of the measured pressure curve of the melt inside the nozzle of the injection molding machine into a time-corrected pressure curve  $p_{mk}$  is possible, which corresponds to a pressure measurement curve at constant flow rate.

As for the virtual events, the real events  $E_{mach}$  can be determined by differentiating the measured pressure signal. For example, for the case shown in Fig. 6, five events can be identified, as shown in Fig. 7.

In Step 8, the real event pattern is generated as described by  $M_m (E_{mach 1}, \dots, E_{mach m})$ .

A typical pattern consists of  $m$  real events  $E_{mach i}$ , which are associated with the characteristic event points of the part geometry. Each real event is assigned to a machine time and a screw position.

$E_{mach i}(t_{mach i}, p_{mach i}, s_{mach i})$  is a vector with three components: the machine time  $t_{mach i}$ , the screw position  $s_{mach i}$ , the measured real melt pressure  $p_{mach i}$  at the time when the event occurs.

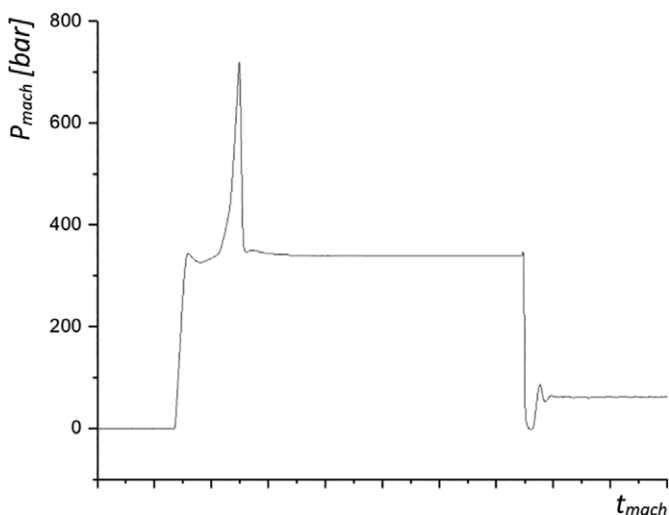


FIG. 6. Measured melt pressure signal across machine time.

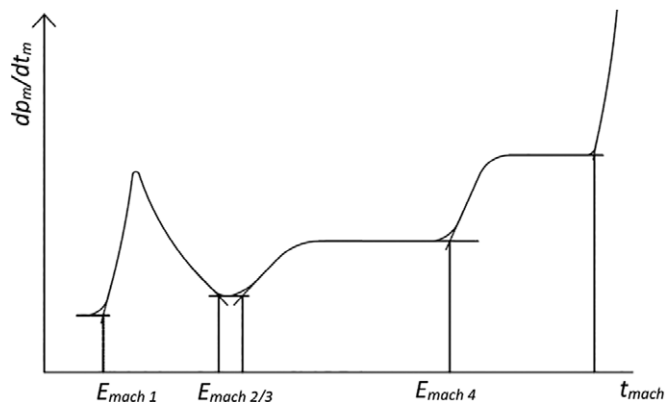


FIG. 7. Five events identified from a measured melt pressure in accordance with the machine time.

Plotted against time, all events form an individual and unique real event pattern (Fig. 8). The pattern describes the relative assignment of all measured events occurring during filling phase.

### Stage 3: Mapping a Simulated Filling Process to a Real Injection Molding Process

Stage 3 consists of six steps: Steps 9–14. In this stage, the simulated process and the real injection process are mapped, virtual and real event patterns are matched and virtual events are assigned to real events.

In this article, the method for determining the flow front position is based on the idea of mapping a simulated filling process to a real injection molding process. The mapping takes place at the event points. The “matching” of the form part-specific pattern to the real event pattern of the filling process, represents the actual mapping process. It cannot be assumed that after identification, the patterns are identical to each other because they differ, for example, due to deviations between machine setting and simulation boundary conditions. Similarly, it cannot be assumed that the patterns have the same size. Depending on the location of the pressure sensor or the scope of the simulation, the patterns might have different numbers of events. Because of this, the proposed method should have a function for transforming the patterns until they can be matched.

In Step 9, for the above purpose, both, the form part-specific event pattern  $M_s$  and the real event pattern  $M_m$  are transferred to an “allocation unit.” The purpose of the allocation unit is to match either whole event patterns or at least parts of them. By matching patterns, the virtual events can be assigned to the real events.

In Step 10, after the process matching, individual virtual events are assigned to real events. Based on the assignment, the melt front position (a component from the virtual event vector  $E_{sim}$ ) can be determined to the respective screw position (a component from the real event vector  $E_{mach}$ ).

In Step 11, the flow front velocity can then be determined on the basis of the time when these events occur.



FIG. 8. Real event pattern  $M_m$ .

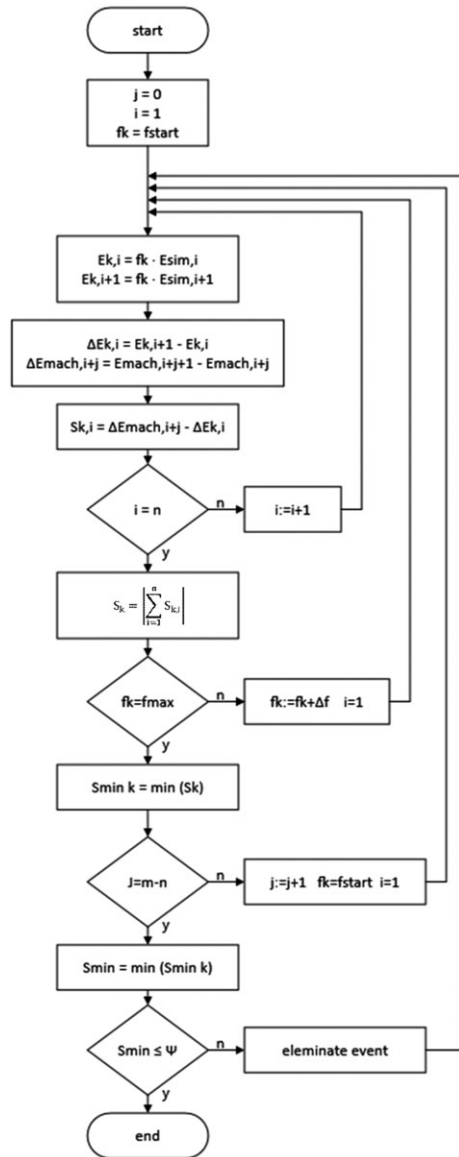


FIG. 9. Matching algorithm.

In Step 12, machine-independent parameters such as melt viscosity, shear rate, and so forth can be finally determined.

In Step 13, a set of machine-independent parameters, which delivers the best form part quality can be stored. If a machine change, these parameters can be used in Step 14 to recalculate the new setting of the machine parameters such as pressure curve, flow rate, and so forth.

**Matching the Form Part-Specific Pattern with the Real Event Pattern.** In Step 9 (the allocation unit), a matching algorithm will be carried out with iteration loops, as shown in Fig. 9.

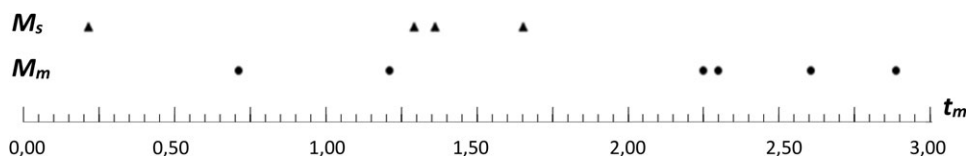


FIG. 10. Real event pattern and form part-specific event pattern before scaling.

In the inner loop of the algorithm, the form part-specific event pattern  $M_s$  is transformed. The scaling factor  $f_k$  passes through a total of  $k$  transformations between  $f_{start}$  and  $f_{max}$  with the scaling increment of  $\Delta f$ . Equation 1 shows how the scaling increment is determined.

$$\Delta f = \frac{f_{max} - f_{start}}{k} \quad (1)$$

For each transformation, a new pattern  $M_k$  is calculated from the pattern  $M_s$  and it is attempted to align with the real event pattern  $M_m$ . For this purpose, two adjacent virtual events  $E_{sim\ i}$  and  $E_{sim\ i+1}$  of the form part-specific event pattern are multiplied by the scaling factor  $f_k$  and then the difference in time of the scaled virtual events is calculated. Subsequently, the deviation  $S_{k,i}$  is determined between the previously calculated time intervals in the form part-specific event pattern and the real event pattern. From the absolute value of the sum of all individual deviations of the scaled pattern with the measured events, the total deviation for the respective scaling iteration is calculated. The inner loop is repeated  $k$  times with the scaling factor  $f_k$  being incremented by  $\Delta f$  each time. The smallest (pattern) deviation of all transformations  $S_{min\ k}$  is searched and recorded at the iteration  $k_{min}$ . Figure 10 depicts a form part-specific event pattern  $M_s$  and a real event pattern  $M_m$  plotted against the machine time  $t_m$ , before  $M_s$  undergoes  $k$  transformations. In the case of the number of events  $n$  of the virtual event pattern is not equal to the number of events  $m$  of the real event pattern, each virtual event  $E_{sim\ i}$  is displaced by the index  $j$  into a real event  $E_{mach\ i+j}$  in a further (higher level) iteration loop and then, all transformations are performed to find out at which displacement  $j_{min}$  the best matching (at the smallest pattern deviation) is achieved. This higher iteration loop is repeated  $(m-n)$  times until all possible displacements have been performed.  $S_{min}$  at the displacement  $j_{min}$  is searched and recorded. In a further step of the algorithm, a condition is tested to verify whether the smallest total deviation over all displacements  $S_{min}$  lies within a specified error bound  $\Psi$ . If this is not the case, single events can be eliminated and the entire process in the outer loop has to be repeated until the above condition is met.

The transformed form part-specific event pattern  $M_{s,j}$  is shown in Fig. 11 after it has undergone three higher level iterations with  $j = 0 \dots 2$ —each at the transformation  $k = k_{min}$  with the smallest (pattern) deviation. As can be seen, for pattern  $M_{s,j = 1}$ , the best alignment to  $M_m$  (with the smallest deviation  $S_{min}$ ) is made.

#### Assigning Virtual Singular Events to Real Singular Events and Determining the Flow Front Position.

Figure 12 shows the assignment of the virtual and the real events from the matched pattern. The assignment allows the real event vectors  $E_{mach\ i+j}$  at transformation  $k = k_{min}$  and displacement  $j = j_{min}$  to be expanded by the components  $x_{sim\ i}$ ,  $y_{sim\ i}$ , and  $z_{sim\ i}$  (positions of all nodes, along the melt front lies) of the assigned virtual event vectors  $E_{sim\ i}$ . Thus, the melt front position is consequently associated with machine time  $t_{mach\ i+j}$  and the screw position  $s_{mach\ i+j}$  (Eq. 2).

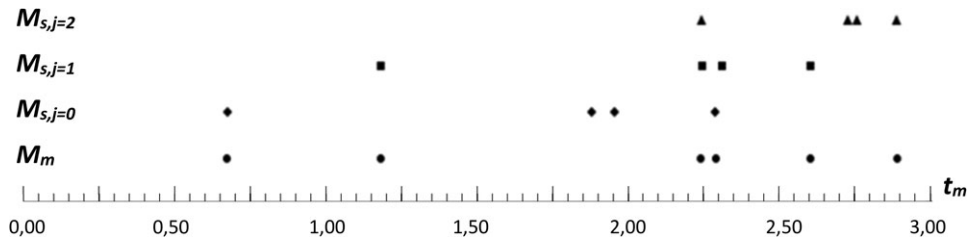


FIG. 11. Real event pattern and form part-specific event patterns after scaling and displacing.

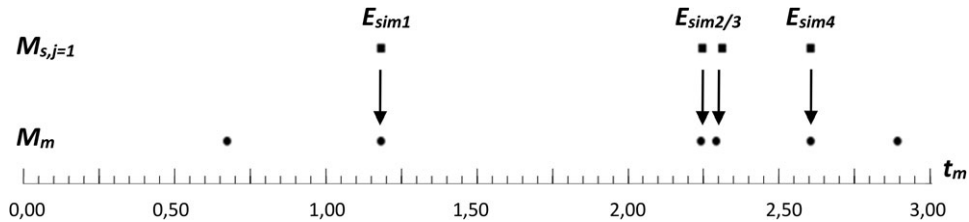


FIG. 12. Assigning virtual events and real events.

$$E_{sim\ i} \rightarrow E_{mach\ i+j} \quad (2)$$

for  $k = k_{min}, j = j_{min}$  and  $S_{min} \leq \Psi$

The real event vector  $E_{mach\ i+j}$ , expanded by the components of the virtual event vector assigned is expressed by  $E_{mach\ i+j}$  ( $t_{mach\ i+j}, p_{mach\ i+j}, S_{mach\ i+j}, x_{sim\ i}, y_{sim\ i}, z_{sim\ i}, h_{sim\ i}$ ).

**Determining Machine Independent Parameters.** By the consideration of two successive and assigned event vectors  $E_{mach\ i+j}$  and  $E_{mach\ i+j+1}$ , the mean flow front velocity of the melt  $v_i$  Eq. 3, as well as the increase in melt pressure  $\Delta p_i$  Eq. 4 are calculated between these events.

$$v_i = \frac{x_{sim\ i+1} - x_{sim\ i}}{t_{mach\ i+j+1} - t_{mach\ i+j}} \quad (3)$$

$$\Delta p_i = p_{mach\ i+j+1} - p_{mach\ i+j} \quad (4)$$

From the calculated flow front velocity and the increase in melt pressure (together with information on the flow channel geometry  $h_{sim\ i}$ ), based on the equation of Hagen–Poiseuille, machine-independent parameters such as the wall shear stress  $\tau_i$ ,

the shear rate  $\dot{\gamma}_i$ , and the melt viscosity  $\eta_i$  expressed in Eqs. 5–7, can be derived between the event points [9, 24].

$$\tau_i = \frac{\Delta p_i \cdot h_{sim\ i}}{2 \cdot (x_{sim\ i+1} - x_{sim\ i})} \quad (5)$$

$$\dot{\gamma}_i = 0,772 \cdot \frac{6 \cdot v_i}{h_{sim\ i}} \quad (6)$$

$$\eta_i = \frac{\Delta p_i \cdot h_{sim\ i}^2}{12 \cdot (x_{sim\ i+1} - x_{sim\ i}) \cdot v_i} \quad (7)$$

## EXPERIMENTAL

Two different form part geometries with different characteristics in terms of the flow path are used to demonstrate and validate the new proposed method. A “step plate” as shown in Fig. 13 is selected as the first case study.

This plate is with sprue bar, lateral dovetail gate, and three-step varying wall thickness over the flow path. The second case study is a symmetrical “stack box,” frontal centrally injected with one-side recess and almost constant wall thickness over the flow path as shown in Fig. 14.

The step plate represents an idealized one-dimensional flow front course. The stack box represents the multidimensional flow course.



FIG. 13. Step plate.

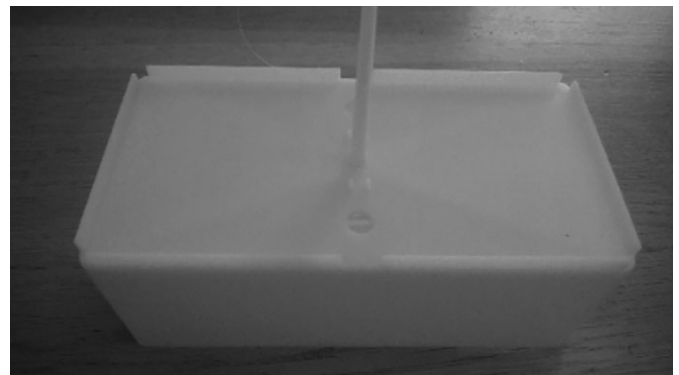


FIG. 14. Stack box.



FIG. 15. Form part geometry of the step plate.

#### Simulation

For the form part geometries, Autodesk Moldflow 2016 was selected to perform the simulation to determine melt flow pattern as well as a virtual pressure curve. In order to get precise results, it is necessary to use a small element size in the three-dimensional (3D) mesh. To obtain a high-quality simulation, mesh elements with unsuitable aspect ratios have been manually adjusted.

Figure 15 shows the meshed part geometry of the step plate with its three times varying wall thickness over the flow. The base area of the step plate is  $120 \times 60 \text{ mm}^2$ . For the simulation, the form part geometry is imported as a “step file.” A mesh with the element size 1 mm is generated as a 3D solid model with eight layers above the wall thickness (677,859 elements).

Figure 16 shows the symmetrical part geometry of the stack box with one-sided recess and a constant wall thickness of  $h = 1.5 \text{ mm}$ .

The base area of the stack box is  $160 \times 75 \text{ mm}^2$ . For the simulation, the part geometry is imported as a “step file” and a mesh with the element size 1.5 mm is generated as a 3D solid model with four layers above the wall thickness (662,399 elements). The mold filling pattern is simulated with a mold surface temperature of  $30^\circ\text{C}$ , a melt temperature of  $250^\circ\text{C}$ , and a volumetric flow rate of  $25 \text{ ccm s}^{-1}$ .

In both simulations, the selected resin is an ABS Terluran GP-22 (BASF). The switchover from filling phase to holding pressure phase is performed at 98% of the volumetric filling. The viscosity dependence is expressed through the Williams–Landel–Ferry

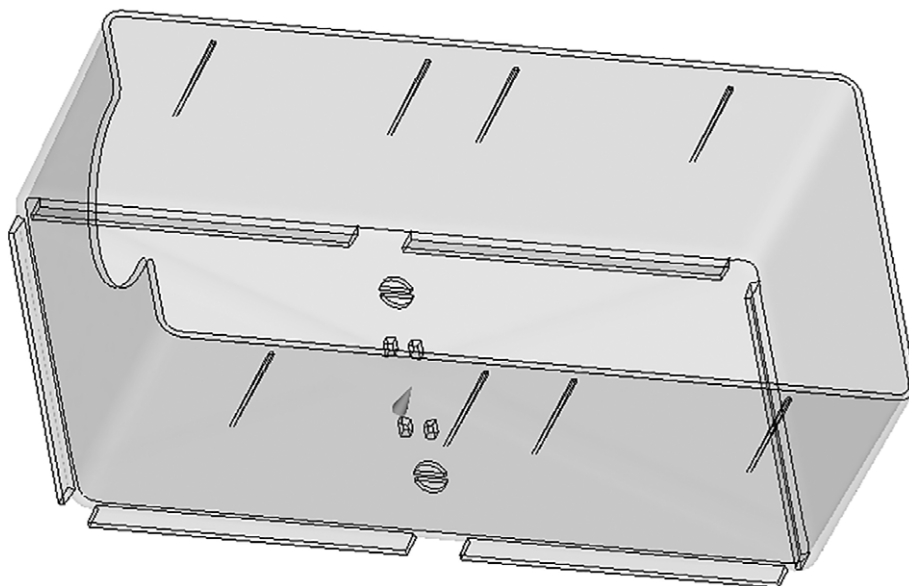


FIG. 16. Form part geometry of the stack box.



FIG. 17. Test setup with molder and mold for the step plate.

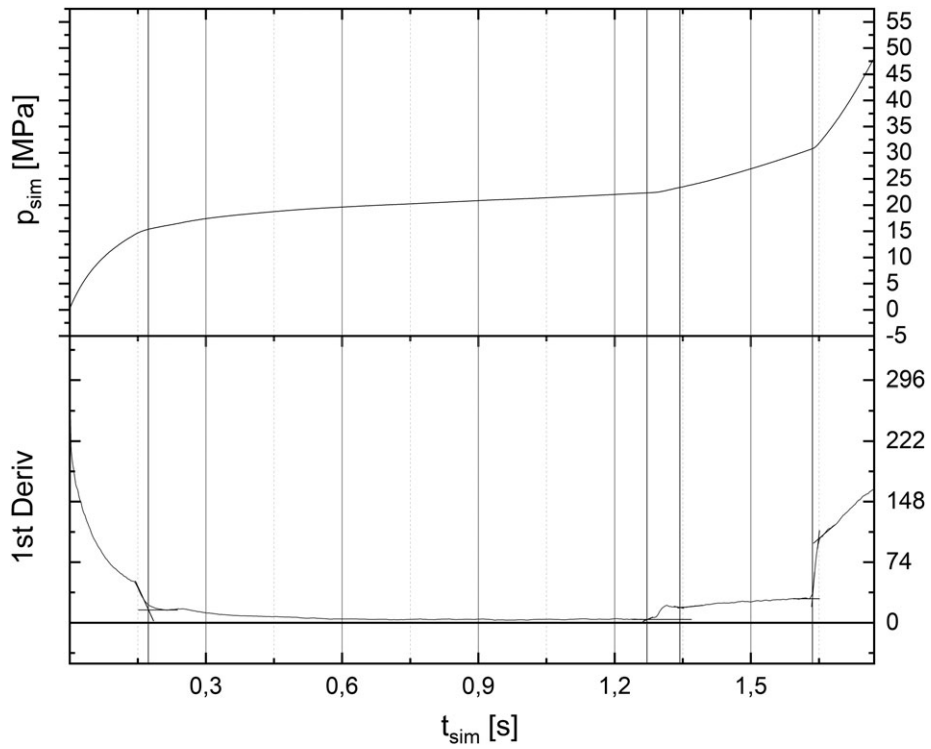


FIG. 18. Step plate: determination of virtual events.

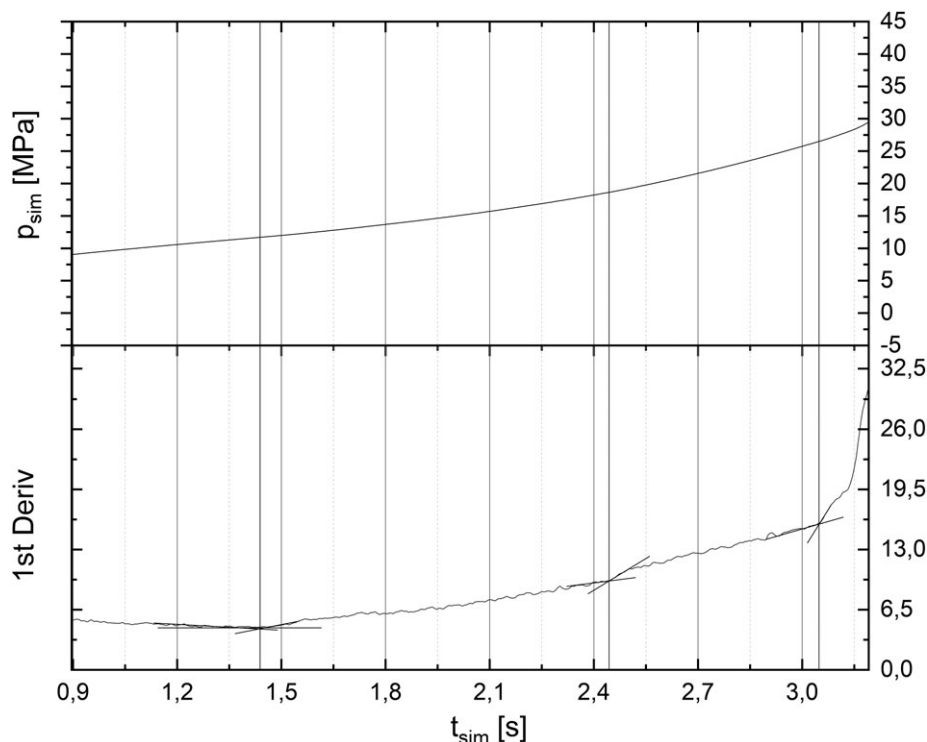


FIG. 19. Stack box: determination of virtual events.

cross model [25] and the required resin properties are obtained using the simulation software's database.

#### Injection Molding Test

The injection molding tests took place on a Battenfeld HM 800 machine with a 30 cm screw diameter, as shown in Fig. 17. The closed-loop controlled injection unit ensued at a constant volumetric flow rate of  $15 \text{ cm}^3 \text{ s}^{-1}$  for the step plate and  $25 \text{ cm}^3 \text{ s}^{-1}$  for the stack box, at a melt temperature set to  $250^\circ\text{C}$  and mold temperature to  $30^\circ\text{C}$ . An ABS Terluran GP-22 was used as the material. The melt pressure during the filling phase was measured using a single pressure sensor located in the front of the screw (mounted in the nozzle of the injection unit) with a resolution of 2 ms per reading.

#### Event Patterns

**Analysis.** The analysis of the differentiated form part-specific pressure curves determines the part-specific event patterns (Figs. 18 and 19), consisting of four virtual event vectors for the step plate (Table 1) and three event vectors for the stack box (Table 2). The virtual event vectors have the following components: virtual event time, melt front position, and melt channel geometry.

TABLE 1. Step plate: form part-specific event pattern.

	$t_{\text{sim}}$ (s)	$x_{\text{sim}}$ (mm)	$h_{\text{sim}}$ (mm)
$E_{\text{sim } 0}$	0.173	0	4.0
$E_{\text{sim } 1}$	1.270	72.5	4.0
$E_{\text{sim } 2}$	1.340	75.8	2.0
$E_{\text{sim } 3}$	1.640	112.5	1.0

The analysis of the differentiated measured pressure signal (Figs. 20 and 21) provides the real event patterns consisting of six event vectors for the step plate (Table 3) and three event vectors for the stack box (Table 4). The real event vectors have the following components: machine time, melt pressure, and screw position.

#### Matching and Assignment

The matching of the patterns and the assignment of the events ensues as described above by means of a transformation as well as a displacement of the events. The matching algorithm passes an interval of  $f_{\text{min}} = 0.1$  to  $f_{\text{max}} = 10$  for a scaling increment of  $\Delta f = 0.01$ .

For the step plate, the algorithm determines the best matching of the patterns at a stretching factor  $f_k = 0.97$  and a displacement  $j_{\text{min}} = 1$  with a total deviation of the patterns  $S_{\text{min}} = 0.00299$  s. According to Eq. 2 and with  $j_{\text{min}} = 1$ , four virtual event  $E_{\text{sim } i}$  can be assigned to four real events,  $E_{\text{mach } i+j}$  ( $E_{\text{sim } 0}$  to  $E_{\text{mach } 1}$ ,  $E_{\text{sim } 1}$  to  $E_{\text{mach } 2}$ , ...). The two real events,  $E_{\text{mach } 0}$  and  $E_{\text{mach } 6}$  have no correspondent virtual events and therefore are not required for the further consideration. For the stack box, the best matching is obtained with a stretching factor of  $f_k = 0.90$  and a displacement of  $j_{\text{min}} = 0$ . At this transformation, the patterns deviate in total  $S_{\text{min}} = 0.001$  s from each other. All three virtual events are assigned to the three real events.

TABLE 2. Stack box: form part-specific event pattern.

	$t_{\text{sim}}$ (s)	$x_{\text{sim}}$ (mm)	$h_{\text{sim}}$ (mm)
$E_{\text{sim } 0}$	1.440	84.0	1.5
$E_{\text{sim } 1}$	2.440	114.0	1.5
$E_{\text{sim } 2}$	3.050	145.0	1.5

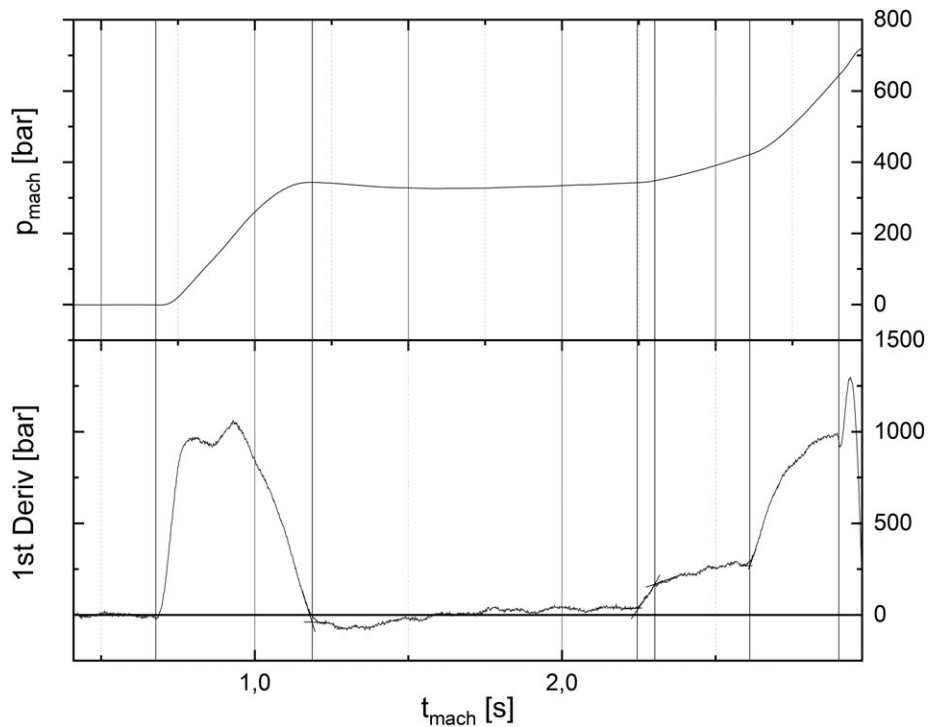


FIG. 20. Step plate: determination of real events.

*Flow Front Velocity*

Tables 5 and 6 list the flow front velocity as well as other machine independent parameters derived from the components of the extended real event vectors. The values shown are average values between the events.

**DISCUSSION**

*Step Plate*

For the visualization of the melt front, the filling pattern (originated through the CAE simulation software) is successively set to the event points assigned to each other.

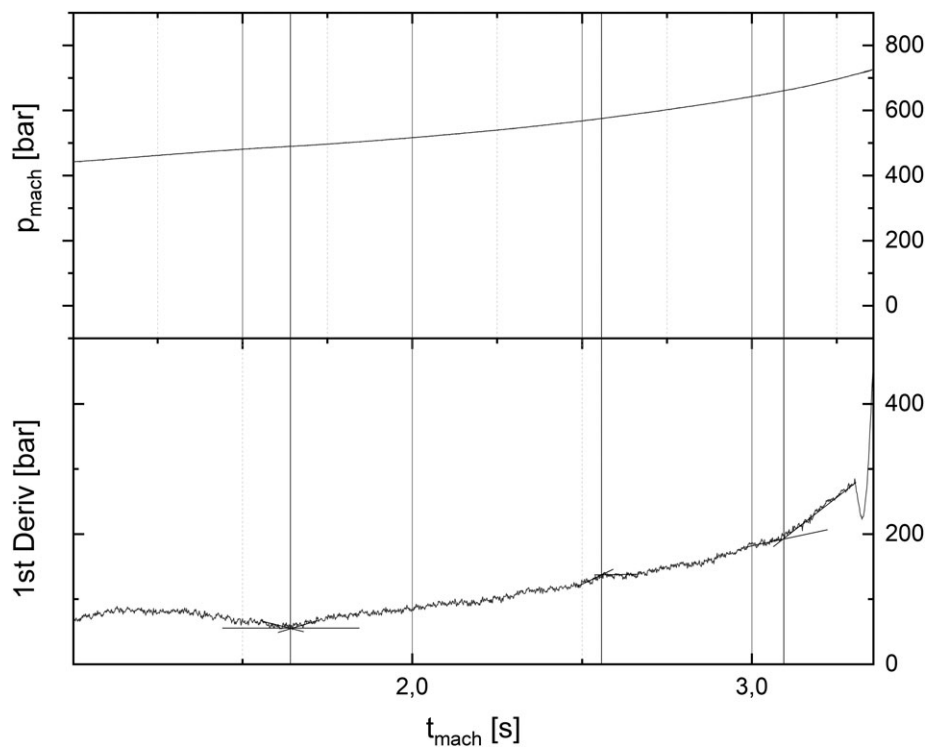


FIG. 21. Stack box: determination of real events.

TABLE 3. Step plate: real event pattern.

	$t_{\text{mach}}$ (s)	$P_{\text{mach}}$ (MPa)	$S_{\text{mach}}$ (mm)
$E_{\text{mach } 0}$	0.680	0.0	14.4
$E_{\text{mach } 1}$	1.190	32.6	25.3
$E_{\text{mach } 2}$	2.250	34.3	47.8
$E_{\text{mach } 3}$	2.300	34.8	48.8
$E_{\text{mach } 4}$	2.610	42.1	55.4
$E_{\text{mach } 5}$	2.900	64.4	61.6

TABLE 4. Stack box: real event pattern.

	$t_{\text{mach}}$ (s)	$P_{\text{mach}}$ (MPa)	$S_{\text{mach}}$ (mm)
$E_{\text{mach } 0}$	1.640	49.0	58.0
$E_{\text{mach } 1}$	2.560	57.6	90.6
$E_{\text{mach } 2}$	3.090	66.1	109.3

TABLE 5. Step plate: machine independent components of event vectors.

	$v_i$ (mm s <sup>-1</sup> )	$\Delta p_i$ (MPa)	$\tau_i$ (kPa)	$\gamma_i$ (1/s)	$\eta_i$ (Pa s)
$E_{\text{mach } 1/2}$	68.4	1.7	47	79.2	457
$E_{\text{mach } 2/3}$	66.0	0.5	303	76.4	3,061
$E_{\text{mach } 3/4}$	118.4	7.3	199	274.2	560

TABLE 6. Stack box: machine independent components of event vectors.

	$v_i$ (mm s <sup>-1</sup> )	$\Delta p_i$ (MPa)	$\tau_i$ (kPa)	$\gamma_i$ (1/s)	$\eta_i$ (Pa s)
$E_{\text{mach } 1/2}$	32.6	8.6	215	100.7	1,648
$E_{\text{mach } 2/3}$	58.5	8.5	206	180.6	879

Figure 22 shows precisely the particular melt front position, at which the form part-specific event  $E_{\text{sim } 0}$  is assigned to the real (measured) event  $E_{\text{mach } 1}$ . The visualization is achieved by setting

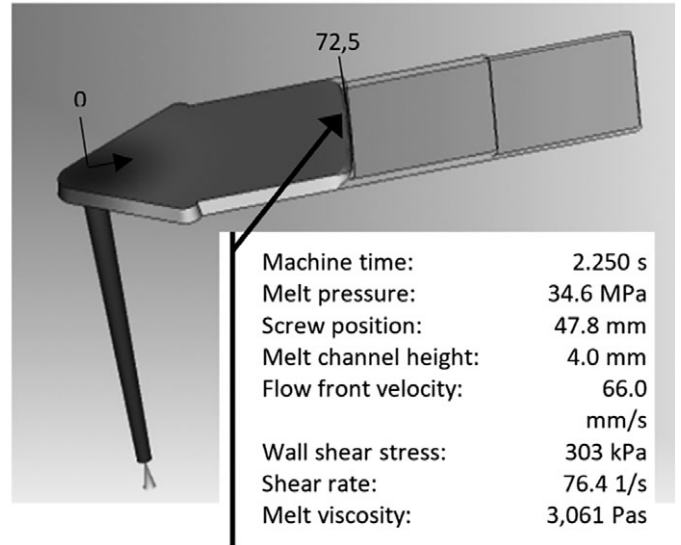


FIG. 23. CAE of the step plate at event  $E_{\text{mach } 2}$ .

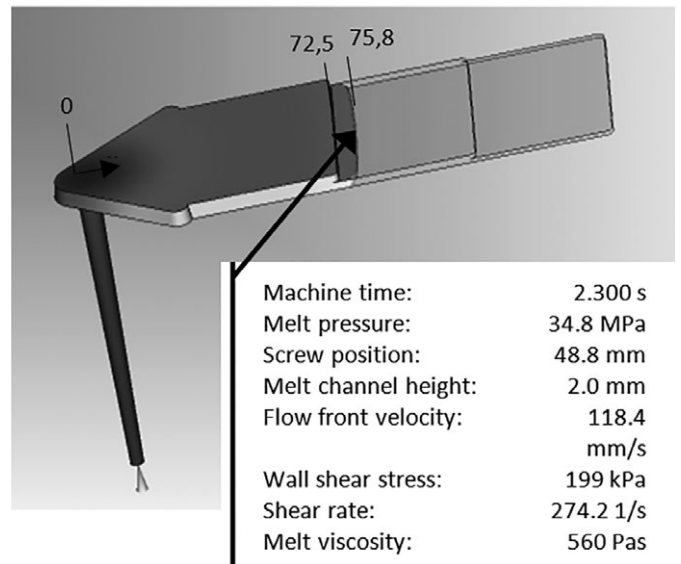


FIG. 24. CAE of the step plate at event  $E_{\text{mach } 3}$ .

the filling pattern to the virtual event time  $t_{\text{sim } 0} = 0.173$  s (component of the virtual event vector). Through the assignment of the events, the virtual event time corresponds to the machine time  $t_{\text{mach } 1} = 1.190$  s (component of the real event vector). As it can be seen in Fig. 22, at this particular event, the melt front has already passed through the sprue bar, hits the upper front plate of the step-plate cavity and is deflected by 90°, while the screw of the injection molder, is at position of  $s_{\text{mach } 1} = 25.3$  mm.

The next event  $E_{\text{mach } 2}$  takes place (at the machine time  $t_{\text{mach } 2} = 2.250$  s) when the melt front “experiences” the first change in the cross-sectional area of the flow channel. It can be visualized by setting the filling pattern to the virtual event time  $t_{\text{sim } 1} = 1.270$  s as shown in Fig. 23. At this event, the screw is at position  $s_{\text{mach } 2} = 47.8$  mm.

After passing through the cross-sectional change, the melt front is fully redeveloped again. This situation is shown in Fig. 24 and

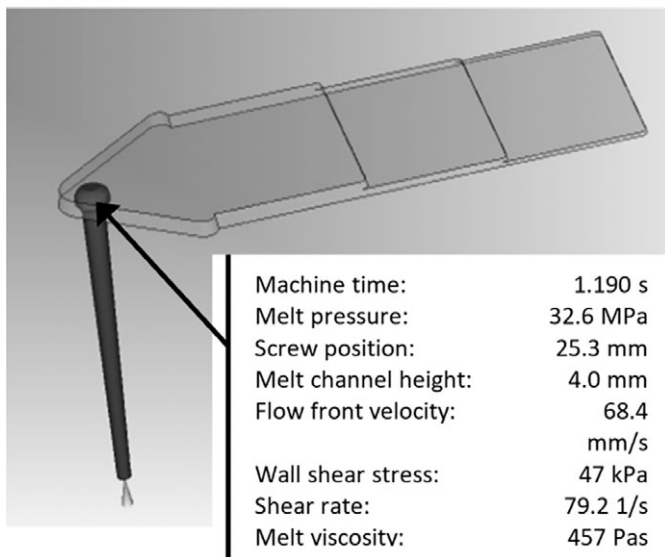


FIG. 22. CAE of the step plate at event  $E_{\text{mach } 1}$ .

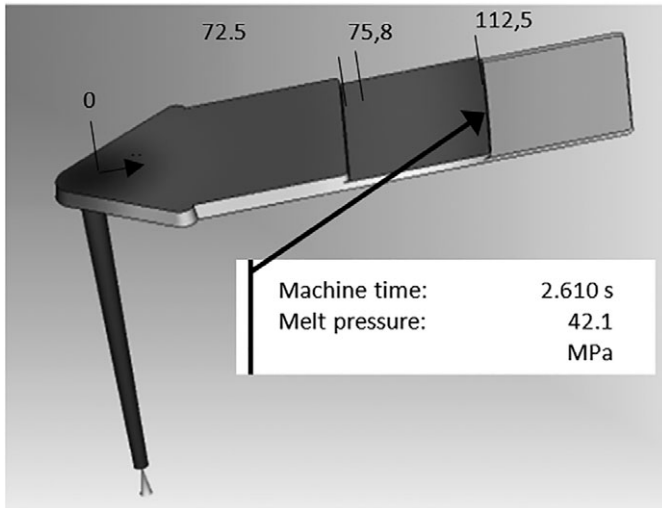


FIG. 25. CAE of the step plate at event  $E_{mach\ 4}$ .

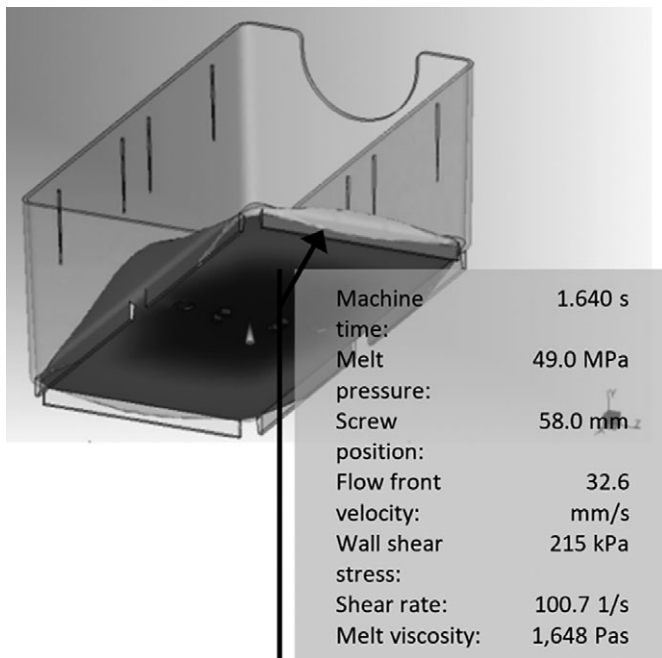


FIG. 26. CAE of the stack box at the event  $E_{mach\ 0}$ .

occurs at the machine time of 2.300 s and a screw position of 48.8 mm. A final event occurs at 2.610 s, when the melt front passes the second change in cross section toward the flow direction. Here, the screw of the injection unit is at position 55.4 mm as shown in Fig. 25.

### Stack Box

Figure 26 shows the arrival of the melt front at event point  $E_{mach\ 0}$ . Once the base plate of the stack box cavity has been filled through the central gate (located at the middle of the front side), the melt front reaches the base of the downward pointing bottom rim at the machine time of 1.640 s. At this point in time, the screw is at position 58.0 mm. The pressure measured is

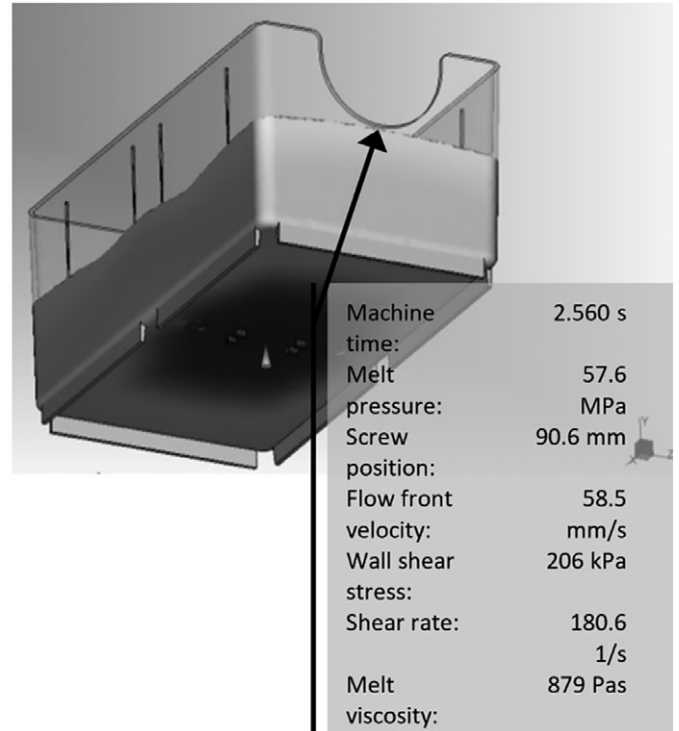


FIG. 27. CAE of the stack box at the event  $E_{mach\ 1}$ .

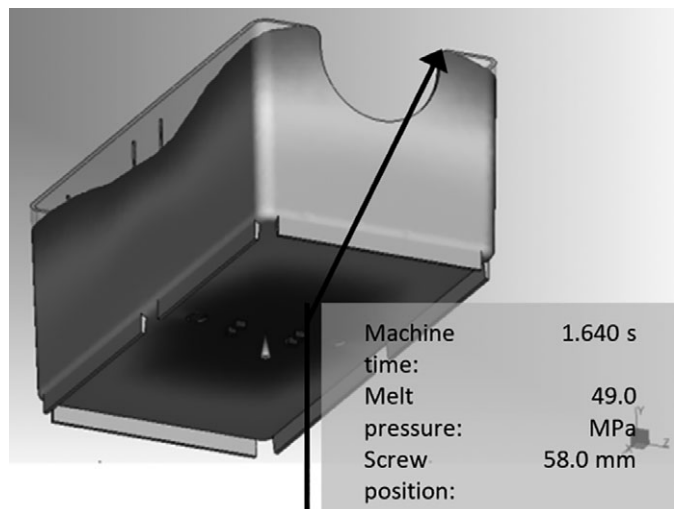


FIG. 28. CAE of the stack box at the event  $E_{mach\ 2}$ .

49.0 MPa. The flow front velocity is being calculated as 32.6 mm  $s^{-1}$ . The wall shear stress at this section is 215 kPa, the melt viscosity is 1,648 Pa s, and the shear rate is 100.7  $s^{-1}$ .

The next event along the flow path of the melt is at the arrival of the flow front at the one-sided recess (Fig. 27). According to theory, this is where an event point and thus a disproportional change in the pressure loss could be expected, because the recess can be perceived (from the perspective of the melt front) as a flow obstacle. However, compared with an event occurring at a location, when the melt front is, for example, redirected at an angle of 90° or passes through a (sharp) cross-sectional change, hitting a (semicircular) flow obstacle at a constant flow channel height has

relatively low influence on the pressure loss. It is impressive that despite such a relatively small impact, both the virtual event  $E_{\text{sim } 1}$  and the real event  $E_{\text{mach } 1}$  could clearly be identified, matched, and assigned and the relationship between the flow front location and the machine time at 2.56 s (respectively, the screw stroke at 90.6 mm) is determined.

At the last event, the flow front reaches the end of the flow channel, first at the side with the one-sided recess. As shown in Fig. 28, the screw is in position 109.3 mm at an injection time of 3.09 s.

It should be pointed out that in these experimental studies, no specific measuring devices (sensors) within the cavity of the mold were used for locating the melt front position during filling phase. From the theoretical analysis and experimental study, it can be seen that:

- I. In both the real injection molding process and the virtual models of the injection process—singular events exist and these events can be identified.
- II. Singular events occur in the form of “event groups.” The sequence of all events from both the real injection molding process and the virtual models of the injection process can be analyzed to identify pattern.
- III. The pattern identified from the virtual models of the injection molding process describes the relative assignment of all events occurring during a virtual filling phase and is considered as the fingerprint of the form part.
- IV. The pattern identified from the real injection molding process describes the relative assignment of all measured events occurring during filling phase as the melt front progresses from the sensor position to the end of the flow path.
- V. By matching the form-part specific event pattern with the real event pattern virtual and real events can be assigned, and the relationships between injection time, screw location, and melt front position can be established.
- VI. Furthermore, the relation between assigned events can be proven by visualizing the filling pattern at the event sites, where simulated virtual events and measured real events are superimposed. At this particular event sites, the filling patterns regularly show flow front locations where events could be expected.
- VII. Finally, it can be shown that through the knowledge of the relationships between melt front locations, injection time, and the geometry of the form part, machine independent parameters such as the melt front velocity, wall stress, shear rate, and melt viscosity could be determined.

## CONCLUSIONS

- I. An innovative method has been proposed, designed, and developed for determining the flow front velocity of a plastic melt in relation to the screw position by using only one single pressure sensor located outside the mold.
- II. This new method is based on the idea of mapping a simulated filling process to a real injection molding process.
- III. The results of the simulation analysis and experimental evaluation show that the proposed method is effective for determining the flow front position and the resulting flow front velocity of the melt on the entire flow path.
- IV. The two case studies have provided the evidences that the new method offers great potential to future process control strategies based on machine independent parameters such as constant melt front velocity or constant melt viscosity during filling phase.

- V. Because the method dispenses with any sensor technology within the mold, it can be used for any existing applications without complex and expensive retrofitting existing molds.
- VI. The new method can also be used to automatically perform the machine and could be an essential component on the way to autonomous injection molding.
- VII. Since a primary requirement for matching the event patterns is the use of an algorithm with functional methods for transforming and assigning pattern and pattern fragments, further research of new matching algorithms would be desirable for future use of the presented method.

## NOMENCLATURE

$A_b$	Cross-sectional area of screw
$A_m$	Cross-sectional area of flow channel
$D$	Diameter of screw
$E$	Singular event
$E_{\text{mach}}$	Real singular event
$E_{\text{sim}}$	Virtual singular event
$f_k$	Scaling factor
$f_{\text{max}}$	Maximum scaling factor
$f_{\text{min}}$	Minimum scaling factor
$\Delta f$	Scaling increment
$h_{\text{sim } i}$	Information on form part geometry at virtual event time
$j$	Number of displacements
$j_m$	Displacement at the smallest pattern deviation
$k$	Number of transformations
$k_{\text{min}}$	Transformation at the smallest pattern deviation
$L$	Length of the flow channel
$F_i$	Event point
$m$	Number of real events
$M_k$	Transformed event pattern
$M_m$	Real event pattern
$M_s$	Form part-specific event pattern
$n$	Number of virtual events
$p_e$	Melt pressure
$p_{\text{mach}}$	Measured (real) melt pressure
$p_{\text{mk}}$	Time corrected melt pressure
$p_{\text{sim}}$	Form part specific (virtual) melt pressure
$S_{k,i}$	Deviation between events
$S_k$	Deviation between patterns
$S_{\text{min } k}$	Smallest pattern deviation of all transformations
$S_{\text{min}}$	Smallest pattern deviation of all transformations and displacements
$s_{\text{mach } i}$	Position of screw at real event time
$t$	Time for injection
$t_{\text{mach}}$	Machine time
$t_{\text{mach } i}$	Real event time
$t_{\text{sim}}$	Virtual injection time
$t_{\text{sim } i}$	Virtual event time
$T_m$	Melt temperature
$T_{\text{wz}}$	Mold temperature
$v$	Velocity of screw
$V$	Volume form part
$\dot{V}$	Volumetric flow rate
$v_b$	Injection velocity
$v_m$	Melt front velocity
$x_b$	Position of screw
$x_m$	Position of melt front
$x_{\text{sim } i}, y_{\text{sim } i}, z_{\text{sim } i}$	Position of melt front at virtual event time
$\dot{\gamma}$	Shear rate

$\tau$	Wall shear stress
$\Psi$	Specific error bound
$\eta$	Melt viscosity

## REFERENCES

1. T. Brinkmann, *Product Development with Polymers*, Carl Hanser, Munich, Germany (2011).
2. X. Chen, *A Study on Profile Setting on Injection Molding*, Hong Kong University (2002).
3. X. Zhou, Y. Zhang, T. Mao, and H. Zhou, *J. Mater. Process. Technol.*, **249**, 358 (2017).
4. O. Ogorodnyk and K. Martinsen, *Procedia CIRP*, **67**, 380 (2018).
5. C. Bader and S.C. Zeller, *Kunststoffe*, **6**, 46 (2010).
6. C. Bader, K Zeitung, Switzerland, **12** (2013).
7. C. Bader, E. Koenig, and C. Schmidt, *Kunststoffe*, **6**, 46 (2013).
8. T. Osswald, L.S. Turng, and P. Gramann, *Injection Molding Handbook*, Carl Hanser, Munich, Germany (2008).
9. S. Stitz and W. Keller, *Injection Moulding (German)*, Carl Hanser, Munich, Germany (2001).
10. W. Michaeli and A. Schreiber, *Adv. Polym. Technol.*, **28**, 2 (2011).
11. P. Kennedy and R. Zheng, *Flow Analysis of Injection Molds*, Carl Hanser, Munich (2013).
12. Y. Yang, "Injection Molding Control: From Process to Quality," Thesis, Hong Kong University of Science and Technology, Hong Kong (2004).
13. A. Boldizar, J. Kubat, and M. Rigdahl, *J. Appl. Polym. Sci.*, **39**, 63 (1990).
14. X. Chen, L. Zhang, X. Kong, J. Lue, and F. Gao, *Polym. Eng. Sci.*, **50**(7), 1358 (2010).
15. X. Chen, G. Chen, and F. Gao, *Polym. Eng. Sci.*, **44**, 8 (2004).
16. C. Chiu, M. Shih, and J. Wei, *Polym. Eng. Sci.*, **31**, 19 (1991).
17. F. Zhou, K. Yao, X. Chen, and F. Gao, *Int. Polym. Process.*, **24**, 253 (2009).
18. G. Ouyang, X. Li, X. Guan, Z. Zhang, X. Zhang, and R. Du, *Adv. Neural Networks*, **3174**, 169 (2004).
19. H. Zhou, *Computer Modelling for Injection Molding*, John Wiley & Sons, Singapore (2013).
20. Y. Wang, D. Zhou, and F. Gao, *J. Process Control*, **16**, 8 (2008).
21. K.-Y. Jiang, Z. Ji, H. Li, M. Wang, and T.-M. Yu, *Int. Polym. Process.*, **32**, 290 (2017).
22. W. Jong, S. Hwang, C. Wu, C. Kao, Y. Huang, and M. Tsai, *Int. Polym. Process.*, **33**, 255 (2018).
23. G. Menges, W. Michaeli, and P. Mohren, *How to Make Injection Molds*, Carl Hanser, Munich, Germany (1999).
24. S. Kulkarni, *Robust Process Development and Scientific Molding*, Carl Hanser, Munich, Germany (2010).
25. J.F. Agassant, P. Avenas, P. Carreau, B. Vergnes, and M. Vincent, *Polymer Processing*, Carl Hanser, Munich (2017).